Pharmaceutical Research, Vol. 22, No. 10, October 2005 (© 2005)
DOI: 10.1007/s11095-005-6628-y

Research Paper

Airway Identification Within Planar Gamma Camera Images Using Computer Models of Lung Morphology

Jeffry D. Schroeter,[1,6] John N. Pritchard,[2] Dongming Hwang,[3] and Ted B. Martonen[4,5,7]

Received March 30, 2005; accepted June 14, 2005

Purpose. Quantification of inhaled aerosols by planar gamma scintigraphy could be improved if a more comprehensive assessment of aerosol distribution patterns among lung airways were obtained. The analysis of planar scans can be quite subjective because of overlaying of small, peripheral airways with large, conducting airways. Herein, a computer modeling technique of the three-dimensional (3-D) branching structure of human lung airways was applied to assist in the interpretation of planar gamma camera images.
Methods. Airway dimensions were derived from morphometric data, and lung boundaries were formulated from scintigraphy protocols. Central, intermediate, and peripheral regions were superimposed on a planar view of the 3-D simulations, and airways were then tabulated by type, number, surface area, and volume in each respective region.
Results. These findings indicate that the central region, for example, consists mostly of alveolated airways. Specifically, it was found that alveolated airways comprise over 99% of the total number of airways, over 95% of the total airway surface area, and approximately 80% of the total airway volume in the central region.
Conclusions. The computer simulations are designed to serve as templates that can assist in the interpretation of aerosol deposition data from scintigraphy images.

KEY WORDS: computer simulations; drug delivery; gamma scintigraphy; lung morphology; mathematical model.

INTRODUCTION

Aerosol therapy protocols could be improved if inhaled pharmacologic drugs were selectively targeted to regional areas of the lung to elicit optimal therapeutic effects (1–6). This can be accomplished by choosing appropriate aerosol characteristics (e.g., size distribution, density, and shape) and inhalation parameters (e.g., flow rate, tidal volume, and breath hold time) to influence the deposition of inhaled drug particles at preferential sites in the lung (7–10). For example, in the treatment of asthma, inhaled bronchodilators must be delivered to the site of action in the large conducting airways while avoiding deposition in the alveolar region to minimize adverse systemic effects (6,11,12). In contrast, for the treatment of diabetes, it is desirable for inhaled insulin to avoid deposition in the conducting airways and deposit in the alveolated airways for subsequent absorption into the bloodstream (13,14). Because total lung deposition is not a sufficient predictor of clinical response (15), an accurate quantification of inhaled aerosols is essential to measure distribution of drug deposited throughout regions of the lung. Therefore, selective deposition of medicinal aerosols in the lung could be enhanced if a more comprehensive assessment of their spatial distribution patterns was obtained.

A common technique for quantifying aerosol deposition in human lungs is with planar gamma scintigraphy. By measuring the amount of inhaled radiolabeled aerosol that is deposited, images can be obtained of the resulting spatial distribution patterns among airways. However, the interpretation of these images can be quite subjective (16). The planar scans are commonly subdivided into predefined regions of interest, representing the central, intermediate, and peripheral regions of the lung. The ability to differentiate aerosol deposition in large, conducting airways and small, peripheral airways in these regions is somewhat ambiguous because of the overlaying of airways in a planar image (17). Inevitably, this ambiguity is caused by the limitation of the resulting images, which are a two-dimensional (2-D)

[1] Curriculum in Toxicology, University of North Carolina, Chapel Hill, North Carolina, USA.
[2] 3M Health Care, 1 Morley Street, Loughborough, LE11 1EP, UK.
[3] Microelectronics Division, IBM Corporation, Research Triangle Park, North Carolina, USA.
[4] Experimental Toxicology Division, NHEERL, ORD, U.S. Environmental Protection Agency, Research Triangle Park, North Carolina, USA.
[5] Division of Pulmonary Diseases, Department of Medicine, University of North Carolina, Chapel Hill, North Carolina, USA.
[6] Present address: CIIT Centers for Health Research, Six Davis Drive, P.O. Box 12137, Research Triangle Park, North Carolina 27709-2137, USA.
[7] To whom correspondence should be addressed. (e-mail: martonen.ted@epa.gov)

projection of a three-dimensional (3-D) distribution, in accurately relating deposition patterns to actual lung structures and thereby assessing regional lung deposition.

In this study, a 3-D computer model of the branching airway network of human lungs was developed to compliment laboratory investigations involving the quantitative measurement of aerosol deposition using planar gamma camera images. The computer models were designed to assist in the analysis of planar scans by identifying individual airways on a generation by generation basis in regional areas of the lung. In this way, a complete mapping of the airways in each region was obtained. The novel approach presented herein uses a projection of 3-D computer simulations of the lung airway structure so that a frontal planar view was obtained. The result was a 2-D image of lung airways in the anterior–posterior direction, in the same manner that planar gamma cameras are used to measure activity in the airways of patients' lungs. Then a partition delineating the different regions was superimposed on the computer simulations to distinguish airways in each respective region. This is an extension over previous efforts (18,19) in which 2-D computer simulations were used to model the airway structure. This 3-D approach overcomes the limitation of 2-D models in accurately simulating the actual shape of the lung, the same limitation that planar images suffer from fully representing the distribution of aerosol deposited in the lung.

The development of computer models to compliment scintigraphy analyses involves (1) computation of the spatial coordinates of each individual airway within the entire network, (2) a mathematical description of a bounding surface representing the lung periphery, (3) the use of computer graphics principles for the visualization of the complex airway structures, and (4) a method of tabulating airways that is compatible with clinical imaging procedures. The bounding surface was defined based on examination of the outer margins of human lungs from scintigraphy images, so that when the airway structure was allowed to develop within, a complete anatomically accurate mapping of the airways was obtained. The resulting computer simulations were then designed to serve as templates, so that when used in conjunction with the tabulation of airways, they can assist in the interpretation of human test data.

MATERIALS AND METHODS

The key factors for the development of anatomically accurate 3-D lung airway models for gamma scintigraphy analyses are a representation of the *exterior* surface of the lung and the formation of its *interior* airway structure. Previous studies have shown that morphologies based on simplified idealized models are aphysical and are therefore limited in their effectiveness with scintigraphy protocols (18,20,21). For an accurate assessment of airway distributions, a morphology has been developed such that the airway networks are confined within mathematically defined boundaries representing lung surfaces. The advantage of using computer-modeling techniques is that information on airway composition can be extrapolated back to the original lung structure. Therefore, if the computer model of the lung airway network accurately simulates the actual airway structure of the patient, then the resulting planar view of the computer simulations will provide a reasonable template to interpret airway activity in the gamma camera scan. In this section, the development of the morphological model of lung airways and the partitioning of scintigraphy scans for the analysis of gamma camera data are discussed.

Development of Lung Morphology

To describe the physical framework of lung airways, the spatial coordinates of each individual airway within the entire network must be computed. By assuming a dichotomous branching system composed of 24 generations beginning with the trachea (generation 0) and ending with the alveolar ducts (generation 23), the bifurcating system of airways was systematically constructed. An individual airway, represented as a cylindrical tube, was uniquely defined by its length and diameter. The placement of airways was then defined by their orientation angles, which consists of a branching angle between two identical airways, and a gravity angle, which is a measure of the rotation of airways at bifurcations. The airway parameters for this study were taken from Martonen *et al.* (21), with orientation angles being an amalgam of results from asymmetric morphology studies (22–24). A mean value for each parameter was defined for every generation so that the airway network was then generated via a recursive computer algorithm. The airways comprising generations 0–16 are conducting airways, whereas generations 17–23 represent alveolated airways. These airway parameters can be easily adjusted to account for variations in patient age, lung size, and disease.

In order for the morphological model to be compatible with the analysis of scintigraphy data, a stylized boundary was defined to describe the outer surface of the lung. Because the airway model is being used in the analysis of planar gamma camera scans, it is natural to define the outer contour of the lung based on examination of lung outlines from previous planar imaging studies (17–19,25). However, because the morphological model developed herein was based on the 3-D structure of the lung, planar images alone are not sufficient to create an accurate lung boundary. Therefore, we have also used data from transverse and coronal slices of 3-D scintigraphy images to assist in the development of the model (26–28). By incorporating these findings, a volumetric bounding surface was defined that is mathematically simple, yet anatomically realistic enough to simulate conditions found *in vivo*. Specifically, the peripheral walls of the lungs were represented in terms of elliptic cones. The apical and basal surfaces were then formed by truncating the cones with transverse cutting planes to form an enclosed region. The visceral pleura was then defined by dividing this region into two halves using vertical cutting planes that distinctly separate the left and right lungs.

In Fig. 1, a computer simulation of the lung airway network within the stylized boundary is presented. The airways are represented by their longitudinal centerlines and are color-coded by generation; the boundary is shown in dotted white lines. Generations 0–12 are shown so that the complex branching structure inherent within human lungs can be easily discerned. The entire airway network (generations 0–23) can also be shown, but then it is impossible to distinguish individual airways because of their extreme

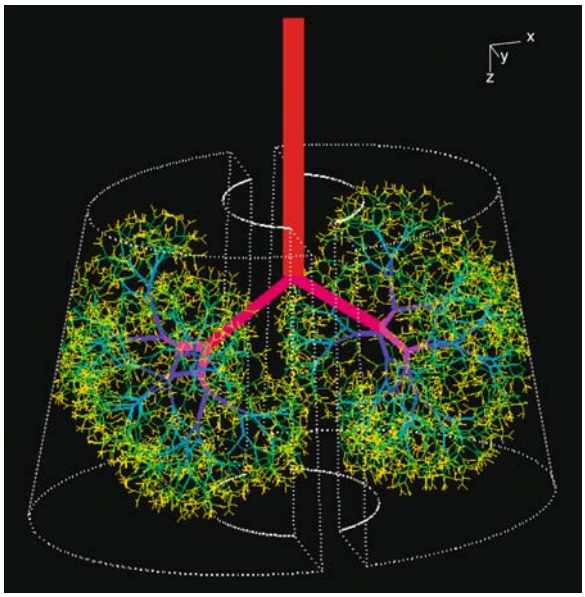

Fig. 1. Computer simulation of generations 0–12 of the airway network (color-coded by generation) with stylized boundary of the outer surface of human lungs defined as truncated, volumetric cones (dotted white lines).

number. The surrounding surfaces, including the apical and basal surfaces, peripheral boundary, and inner cavity boundaries, are clearly visible. The trachea is seen to enter the inner cavity region and branch into the left and right main bronchi. All further airways are void from this region, thus separating the lung into distinctive left and right components. The airways are restricted from exiting the bounded regions to retain the integrity of the surface. If an airway were to occur outside the boundary, it is reflected back inside the region at an equal angle of incidence to the lung surface. Thus, a morphological model is developed to be consistent with scintigraphy protocols, and the lung airway system is reduced to a matrix of points so that the locations of individual airways can be tabulated.

Partition of Gamma Camera Scan

In planar imaging analyses, a template designating different regions of the lung is typically overlaid onto the gamma camera scans. To define the template in experimental practice, the outer contour of the lung must first be determined by a ventilation or perfusion scan (29,30). Once the outer contour is determined, an offset concentric interval circumventing the planar image is defined to designate the peripheral (P) region. Subsequently, another offset interval is nested inside the P region to designate the intermediate (I) region. The remaining portion is designated the central (C) region. Various shapes have been used to delineate these regions (31–35), and the resulting analyses are usually quite subjective.

For modeling applications, these regions must be defined more precisely. The approach presented herein defines the region perimeters in mathematical terms in a similar manner as regions defined in previous experimental investigations (31,34). In Fig. 2, a template of the partition used for theoretical studies of the C, I, and P (CIP) regions is

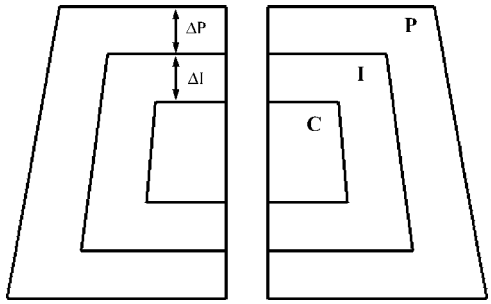

Fig. 2. Partition of a planar gamma camera image template into the respective central (C), intermediate (I), and peripheral (P) regions.

presented. The outline of the P region coincides with a posterior cross-section of the volumetric cones used for the lung boundaries, as seen in Fig. 1 (i.e., the intersection of the plane containing the trachea and main bronchi with a volumetric cone truncated by upper and lower horizontal cutting planes forms the planar trapezoidal shape outlining the perimeter of the P region). The different zones are subdivided so that $\Delta C = \Delta I = \Delta P$, where ΔI and ΔP are the interval widths of the intermediate and peripheral regions, respectively, as indicated in Fig. 2, and $2\Delta C$ is the height of the C region. In this way, the height of the lung region is subdivided equally into the various zones. With this particular subdivision, the CIP regions comprise approximately 15, 33, and 52% of the total surface area of the planar image, respectively. Because the perimeter of the P region is designated to coincide with the outer boundary of the lung, the zones can be scaled accordingly to adapt for various lung sizes. The shapes of the individual zones defined in the model can also be easily altered to adapt to various shapes of CIP regions used in different imaging protocols.

Because the lung airway model is an actual 3-D structure, the template shown in Fig. 2 is overlaid on an anterior projection of the computer simulations. To visualize how the template appears in 3-D, an angular view is presented in Fig. 3 of the CIP regions. The planar trapezoidal shapes representing each region are "tunneled" back through the airway structure along the axis perpendicular to the face of the template to distinctly identify the separate regions in 3-D.

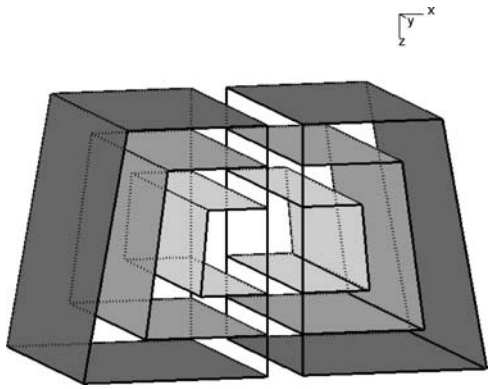

Fig. 3. Angular view of the recessed template from Fig. 2, designed so that 3-D computer simulations of lung airways can be compatible with planar imaging analyses.

RESULTS

The computer model essentially consists of an algorithm to compute the locations of individual airways and the use of computer graphics techniques to render the resulting airway structures. The computations were performed on an SGI (Mountain View, CA) Octane workstation. To view the lung airway network inside the various zones, a planar anterior view of generations 0–12 of the airway network is presented in Fig. 4. The partition delineating the CIP regions is overlaid so that the position of airways with respect to the various regions can be identified. In Fig. 5, an angular view, analogous to Fig. 3, of the airway structure inside the zones is presented so that the penetration of airways with respect to the lung template can be seen. Note that the airways are still enclosed within the lung boundary from Fig. 1, and the template is sized accordingly to encompass the entire lung volume.

The airways of the lung were represented in mathematical terms as a matrix of points, each defined by its respective center of mass, and were systematically tabulated in the CIP regions, as defined in Figs. 2 and 3. The lengths and diameters of the airways were then used to compute the total airway surface area and volume in each region. The degree of alveolation for each airway was determined using the model of the respiratory zone from Weibel (36). The additional surface area and volume from the alveolar sacs were computed using the dimensions of an individual model alveolus, resulting in a cumulative total of 298,450,944 alveoli, an alveolar surface area of 607,347.67 cm^2, and an alveolar volume of 3,133.73 cm^3.

The data in Tables I–IV present the composition of airways in the CIP regions of a gamma camera scan. The tables are organized in the following manner: Tables I and II provide data for the number of airways in each region; Table III provides data for the corresponding airway surface area in each region; and Table IV provides data for the corresponding airway volume in each region. Surface area and volume calculations are included because they may provide more meaningful results than airway counts for use in aerosol deposition studies. The tabular composition of airways by generation in Table I provides the most comprehensive assessment possible in the CIP regions. This detailed airway assessment was also tabulated for airway surface area and volume; for brevity, these data were not shown. Tables II, III, and IV provide a categorization of airways by number, surface area, and volume, respectively. The airways are organized by type, meaning whether they are in the tracheobronchial (TB) compartment, comprising generations 1–16, or in the pulmonary (PU) compartment, comprising generations 17–23, and also include the alveoli. The data are organized into three sections: rows 1–4 show the values in each region for the total (TB + PU) airways, TB airways, PU airways, and the alveoli; rows 5 and 6 show the percentage of TB and PU airways relative to the totals in each region; and

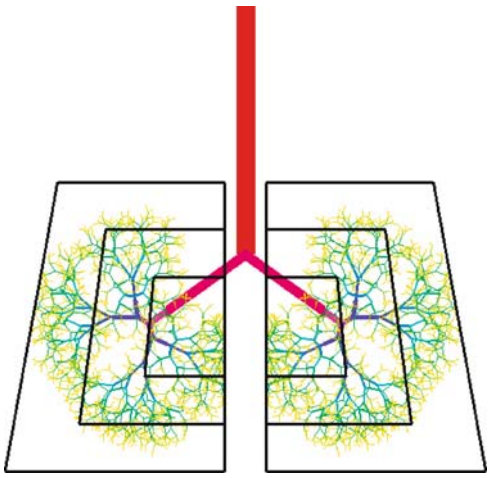

Fig. 4. Planar view of the 3-D airway morphology model (generations 0–12) with overlaid partition.

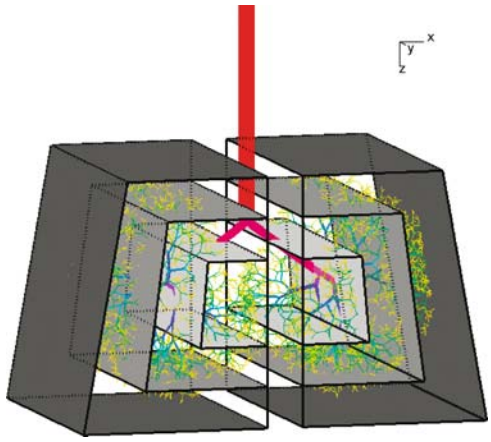

Fig. 5. Angular view of the 3-D morphology model (generations 0–12) inside the template designating the C, I, and P regions.

Table I. Composition of Airways in the Central (C), Intermediate (I), and Peripheral (P) Regions of a Planar Gamma Camera Image

	Partition of scan		
Airway generation	Region C	Region I	Region P
1	2	0	0
2	4	0	0
3	4	4	0
4	8	8	0
5	8	24	0
6	16	32	16
7	32	64	32
8	52	140	64
9	96	252	164
10	196	448	380
11	380	816	852
12	736	1,608	1,752
13	1,452	3,244	3,496
14	2,908	6,360	7,116
15	5,890	12,522	14,356
16	11,800	25,116	28,620
17	23,746	49,986	57,340
18	47,570	99,722	114,852
19	95,416	199,368	229,504
20	190,724	399,044	458,808
21	381,280	798,760	917,112
22	762,674	1,597,874	1,833,756
23	1,526,286	3,197,066	3,665,256

Table II. Categorization of Airways and Alveoli in the Central (C), Intermediate (I), and Peripheral (P) Regions of a Planar Gamma Camera Image

	Partition of scan		
	Region C	Region I	Region P
Total number of airways	3,051,280	6,392,458	7,333,476
Number of TB airways	23,584	50,638	56,848
Number of PU airways	3,027,696	6,341,820	7,276,628
Total number of alveoli	54,284,704	113,703,804	130,462,436
TB/Total	0.0077	0.0079	0.0078
PU/Total	0.9923	0.9921	0.9922
Total airways/N_{Tot}[a]	0.1819	0.3810	0.4371
TB airways/N_{TB}[b]	0.1799	0.3863	0.4337
PU airways/N_{PU}[c]	0.1819	0.3810	0.4371
Alveoli/N_{Alv}[d]	0.1819	0.3810	0.4371

[a] N_{Tot} = cumulative number of airways in C, I, and P regions = 16,777,214.
[b] N_{TB} = cumulative number of TB airways in C, I, and P regions = 131,070.
[c] N_{PU} = cumulative number of PU airways in C, I, and P regions = 16,646,144.
[d] N_{Alv} = cumulative number of alveoli in C, I, and P regions = 298,450,944.

rows 7–10 show the TB + PU airways, TB airways, PU airways, and the alveoli, normalized to their respective totals in the entire lung.

In Fig. 6, computer simulations of the TB and PU airways in the CIP regions of the lung are presented. The left column of Fig. 6 displays only the TB airways, and the right column displays only the PU airways. The trachea and portion of the main bronchi that occur in the inner cavity are not shown. The composite images of rendered airways are restricted to the respective CIP regions in the lung template so that a clear image of the distribution of airways by type and region is obtained. Using these images along with the comprehensive data from Tables I–IV, a direct relation-

Table III. Categorization of Airway and Alveolar Surface Area (cm^2) in the Central (C), Intermediate (I), and Peripheral (P) Regions of a Planar Gamma Camera Image

	Partition of scan		
	Region C	Region I	Region P
Total surface area of airways	20,031.51	41,900.48	47,847.32
Surface area of TB airways	855.91	1,734.97	1,755.96
Surface area of PU airways	19,175.60	40,165.52	46,091.37
Total surface area of alveoli	110,469.36	231,387.22	265,491.04
TB/Total	0.0428	0.0414	0.0367
PU/Total	0.9573	0.9586	0.9633
Total airways/S_{Tot}[a]	0.1825	0.3817	0.4359
TB airways/S_{TB}[b]	0.1969	0.3991	0.4040
PU airways/S_{PU}[c]	0.1819	0.3810	0.4372
Alveoli/S_{Alv}[d]	0.1819	0.3810	0.4371

[a] S_{Tot} = cumulative surface area of airways in C, I, and P regions = 109,779.31 cm^2.
[b] S_{TB} = cumulative surface area of TB airways in C, I, and P regions = 4,346.84 cm^2.
[c] S_{PU} = cumulative surface area of PU airways in C, I, and P regions = 105,432.49 cm^2.
[d] S_{Alv} = cumulative surface area of alveoli in C, I, and P regions = 607,347.67 cm^2.

Table IV. Categorization of Airway and Alveolar Volume (cm^3) in the Central (C), Intermediate (I), and Peripheral (P) Regions of a Planar Gamma Camera Image

	Partition of scan		
	Region C	Region I	Region P
Total volume of airways	170.86	326.05	361.42
Volume of TB airways	34.60	40.64	33.85
Volume of PU airways	136.26	285.41	327.57
Total volume of alveoli	569.99	1,193.89	1,369.86
TB/Total	0.2025	0.1246	0.0937
PU/Total	0.7975	0.8754	0.9063
Total airways/V_{Tot}[a]	0.1991	0.3799	0.4211
TB airways/V_{TB}[b]	0.3172	0.3725	0.3103
PU airways/V_{PU}[c]	0.1819	0.3809	0.4372
Alveoli/V_{Alv}[d]	0.1819	0.3810	0.4371

[a] V_{Tot} = cumulative volume of airways in C, I, and P regions = 858.33 cm^3.
[b] V_{TB} = cumulative volume of TB airways in C, I, and P regions = 109.09 cm^3.
[c] V_{PU} = cumulative volume of PU airways in C, I, and P regions = 749.24 cm^3.
[d] V_{Alv} = cumulative volume of alveoli in C, I, and P regions = 3,133.73 cm^3.

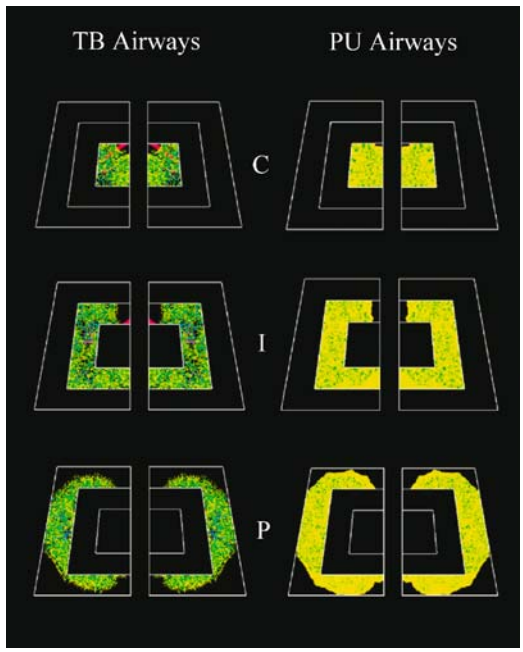

Fig. 6. Computer simulations of a planar view of the lung airways in their respective C, I, and P regions. The left column displays only the tracheobronchial (TB) airways (generations 1–16); the right column displays only the pulmonary (PU) airways (generations 17–23). The airways are color-coded by generation.

ship can be established between activity and lung anatomy to assist in the subjective analysis of scintigraphy data.

DISCUSSION

The data in Tables I–Tables IV and the images from Fig. 6 provide a complete mapping of the entire lung airway structure for planar imaging analyses. One interesting feature to note from these data is that each region contains TB airways, and each region also consists mostly of alveolated airways. Specifically, it was found that the C region, commonly assumed to be composed mostly of large, conducting airways, actually consists of over 99% alveolated airways by number, over 95% alveolated airways by surface area, and approximately 80% alveolated airways by volume. Because the number of airways increases exponentially by generation, the PU airways will typically dominate in number over the TB airways in any specified region. Therefore, it is perhaps more fitting to analyze the composition of airways in each region normalized to their respective totals in the lung. In this case, the C region contains approximately 18% of the PU airways by number, surface area, and volume and approximately 18% of the alveoli. As one might expect, the greatest concentration of PU airways occurs in the P region. Specifically, the P region contains approximately 44% of the PU airways by number, surface area, and volume and approximately 44% of the alveoli. However, the P region also contains a significant fraction of TB airways. Specifically, the P region contains approximately 43% of the TB airways by number, approximately 40% of the TB surface area, and approximately 31% of the TB volume. The P region contains the least amount of volume from the TB airways because the larger proximal airways occur mainly in the C and I regions. These results can be used to more accurately assess aerosol deposition patterns among the CIP regions in a planar scan. These data can also be used to compute the relative proportions of airways found in the P region to those found in the C region (P/C ratio) to assist in the interpretation of the penetration index of inhaled aerosols. For example, considering airway numbers, the P/C ratio is approximately 2.4 for both TB and PU airways. For airway surface area, the P/C ratio is 2.05 for TB airways and 2.4 for PU airways. For airway volume, the P/C ratio is 0.98 for TB airways and 2.4 for PU airways. These ratios can be used to determine the sensitivity of planar imaging in assessing regional deposition.

The advantage of using 3-D models of lung morphology for imaging analyses is that the underlying anatomical structure of the lung is captured. In a previous effort (19), a 2-D model of the lung airways was used to interpret planar images by quantitatively identifying airways in the CIP regions. Although the outer boundary and the delineation of the regions were different than those used in this study, it is still worthwhile to compare the results obtained with the different models. Using the 2-D model, it was calculated that the C region contains approximately 2.8% of the TB airways and approximately 2.1% of the PU airways, whereas the P region contains approximately 79.3% of the TB airways and approximately 82.3% of the PU airways. These numbers are significantly lower in the C region and much greater in the P region than those found in this study. The discrepancy is most likely because of the fact that the 2-D model is not anatomically accurate (i.e., it is impossible for 2-D models to account for lung depth). The airways tend to propagate outward as they bifurcate, thereby increasing their concentration in the P region. This 3-D model, on the other hand, attempts to account for the true shape of the lung by using idealized boundaries defined by elliptical cones and reflecting inward the airways that would intersect the boundary. The purpose of airway reflection is to compensate for the limitations of idealized morphometric airway models in accurately representing lung structure (21). Because the boundary is used to define the outer surface of the lung, airways are reflected in the "peripheral" region of the lung space. Therefore, reflection only occurs at the PU and distal TB airways. However, because the "peripheral" boundary does not directly correspond to the P region of a planar template, the concentration of PU airways can increase in the C and I regions because of the effect of the airways curving around the inner cavity boundary (as seen in the angular view of the airway structure in Fig. 1). Although the airways are located in the "periphery" of the lung space, they can still occur in the C or I region, as seen in Fig. 6. Because planar images are projections of lung activity and do not provide information on lung depth, they cannot distinguish contributions from large airways and overlapping alveolated airways in each of these regions. Therefore, 3-D models can serve as a valuable asset in overcoming this limitation of planar imaging techniques. There is no direct evidence that use of the current 3-D lung structure provides more accurate results than those obtained with the 2-D model. The assumption is that a lung model constructed in the most anatomically realistic fashion possible will yield the most accurate results to compare with clinical data. That being said, it should be noted that there were necessary simplifications in the construction of this model. Specifically, the assumptions of a dichotomously branching system and the idealized boundaries describing the outer contours of the lung were necessary to develop a graphical model capable of recapitulating the entire lung structure in detail. Whereas these assumptions lead to potential limitations with the use of this model, they nevertheless produce a geometry that contains the elements of the complex airway structure necessary to accurately mimic lung shapes.

To improve the discrimination of aerosol deposition in large airways and lung parenchyma, 3-D imaging techniques such as single photon emission computed tomography (SPECT) (37,38) or positron emission tomography (PET) (39,40) can be used. Techniques have been developed to derive information on aerosol distribution by airway generation from SPECT protocols based on simplified anatomical models (28). The approach presented in this study uses a more anatomically accurate computer model to compensate for the limitations of planar images. Although 3-D techniques may provide finer resolution and can provide information on lung volume, planar gamma cameras are still considered practical and valuable tools for assessing total and regional deposition for therapeutic and diagnostic studies. The relative sensitivity of 2-D and 3-D imaging techniques in determining regional deposition can be compared by computing the penetration index of the distribution of activity in the lung (17,41). However, for 2-D imaging techniques, the penetration index will be a sensitive function of the actual

distribution of airways in the C and P regions. By using 3-D computer models of lung airway structures, we are able to tabulate and quantify airways by number, surface area, and volume in the CIP regions. These calculations can then be used to assist in the quantification of deposition patterns with lung anatomy to improve the accuracy of planar imaging studies.

CONCLUSIONS

Planar imaging is compromised by limited resolution because the resulting images represent a sum of airway activity from lung depth along the axis of projection. The interpretation of these images can be quite subjective because of the embedding of small alveolated airways with large conducting airways. It is therefore difficult to relate deposition patterns to lung anatomy because the defined "regions of interest" in clinical applications do not directly correspond with the 3-D structure of the lung. For example, the P region, commonly designated to discern alveolated airways, does not directly correspond with the periphery of the lung volume. In this study, anatomically realistic 3-D computer models of lung airways were developed to assist in the quantification of inhaled aerosols from planar gamma scintigraphy studies. These models allow for the precise identification of individual airways so that a comprehensive tabulation by number, surface area, and volume in the CIP regions can be performed. This geometry, which contains a very high level of detail, can be applied to partition counts of radioactivity per region, thereby enabling a regional mapping of aerosol deposition obtained from planar scintigraphic images. The ability to distinguish different types of airways in regional areas of the lung will assist in the assessment of spatial distribution patterns among lung airways and thereby may lead to improvements in aerosol therapy protocols involving the targeted delivery of inhaled drugs.

In future efforts, this lung geometry will be used in conjunction with mathematical models that predict particle deposition in lung airways. At that point, a detailed analysis can then be undertaken comparing theoretical predictions of aerosol deposition with experimental data from scintigraphy studies using planar scans and 3-D imaging techniques such as SPECT and PET.

DISCLAIMER

The information in this document has been funded wholly (or in part) by the U.S. Environmental Protection Agency. It has been subjected to review by the National Health and Environmental Effects Research Laboratory and approved for publication. Approval does not signify that the contents necessarily reflect the views of the Agency, nor does mention of trade names or commercial products constitute endorsement or recommendation for use.

ACKNOWLEDGMENTS

Jeffry D. Schroeter was funded by the EPA/UNC Toxicology Research Program, Training Agreement CT902908 and CT827206, with the Curriculum in Toxicology, University of North Carolina at Chapel Hill.

REFERENCES

1. M. T. Newhouse and R. E. Ruffin. Deposition and fate of inhaled aerosols. *Chest* **73S**:936–942 (1978).
2. R. E. Ruffin, M. B. Dolovich, R. K. Wolff, and M. T. Newhouse. The effects of preferential deposition of histamine in the human airway. *Am. Rev. Respir. Dis.* **117**:485–492 (1978).
3. G. C. Smaldone, L. Walser, R. J. Perry, J. S. Ilowite, W. D. Bennet, and M. Greco. Generation and administration of aerosols for medical and physiological research studies. *J. Aerosol Med.* **2**:81–87 (1989).
4. P. J. Anderson, E. Garshick, J. D. Blanchard, H. A. Feldman, and J. D. Brain. Intersubject variability in particle deposition does not explain variability in responsiveness to methacoline. *Am. Rev. Respir. Dis.* **144**:649–654 (1991).
5. H. L. Ashworth, C. G. Wilson, E. E. Sims, P. K. Wotton, and J. G. Hardy. Delivery of propellant soluble drug from a metered dose inhaler. *Thorax* **46**:245–247 (1991).
6. J. Lotvall. Inhalation therapy of the future — how will it change the way we treat asthma? *J. Aerosol Med.* **14**(Suppl. 1):S45–S50 (2001).
7. M. Dolovich, M. Vanzieleghem, K. G. Hidinger, and M. T. Newhouse. Influence of inspiratory flow rate on the response to terbutaline sulfate inhaled via a Turbuhaler. *Am. Rev. Respir. Dis.* **137**:433–439 (1988).
8. S. P. Newman, F. Moren, E. Trofast, N. Talaee, and S. W. Clarke. Terbutaline sulfate turbuhaler: effect of inhaled flow rate on drug deposition and efficiency. *Int. J. Pharm.* **74**:209–213 (1991).
9. T. B. Martonen and I. M. Katz. Deposition patterns of aerosolized drugs within human lungs: effects of ventilatory parameters. *Pharm. Res.* **10**:871–878 (1993).
10. T. B. Martonen and I. Katz. Deposition patterns of polydisperse aerosols within human lungs. *J. Aerosol Med.* **6**:251–274 (1993).
11. P. H. Howarth. Why particle size should affect clinical response to inhaled therapy. *J. Aerosol Med.* **14**(Suppl. 1):S27–S34 (2001).
12. P. Zanen, T. L. Go, and J. W. J. Lammers. The optimal particle size for β-adrenergic aerosols in mild asthmatics. *Int. J. Pharm.* **107**:211–217 (1994).
13. B. L. Laube, G. W. Benedict, and A. S. Dobs. Time to peak insulin level, relative bioavailability, and effect of site of deposition of nebulized insulin in patients with noninsulin-dependent diabetes mellitus. *J. Aerosol Med.* **11**:153–173 (1998).
14. I. M. Katz, J. D. Schroeter, and T. B. Martonen. Factors affecting the deposition of aerosolized insulin. *Diabetes Technol. Ther.* **3**:387–397 (2001).
15. J. N. Pritchard. The influence of lung deposition on clinical response. *J. Aerosol Med.* **14**(Suppl. 1):S19–S26 (2001).
16. J. E. Agnew. Characterizing lung aerosol penetration. *J. Aerosol Med.* **4**:237–249 (1991).
17. P. R. Phipps, I. Gonda, D. L. Bailey, P. Borham, G. Bautovich, and S. D. Anderson. Comparisons of planar and tomographic gamma scintigraphy to measure the penetration index of inhaled aerosols. *Am. Rev. Respir. Dis.* **139**:1516–1523 (1989).
18. T. B. Martonen, Y. Yang, and M. Dolovich. Definition of airway composition within gamma camera images. *J. Thorac. Imaging* **9**:188–197 (1994).
19. T. B. Martonen, Y. Yang, M. Dolovich, and X. Guan. Computer simulations of lung morphologies within planar gamma camera images. *Nucl. Med. Commun.* **18**:861–869 (1997).
20. T. B. Martonen, Y. Yang, D. Hwang, and J. S. Fleming. Computer simulations of human lung structures for medical applications. *Comput. Biol. Med.* **25**:431–446 (1995).
21. T. B. Martonen, J. D. Schroeter, D. Hwang, J. S. Fleming, and J. H. Conway. Human lung morphology models for particle deposition studies. *Inhal. Toxicol.* **12**:109–121 (2001).
22. K. Horsfield and G. Cumming. Angles of branching and diameters of branches in the human bronchial tree. *Bull. Math. Biophys.* **29**:245–259 (1967).
23. K. Horsfield, G. Dart, D. E. Olson, G. F. Filley, and G. Cumming. Models of the human bronchial tree. *J. Appl. Physiol.* **31**:207–217 (1971).
24. H. C. Yeh and G. M. Schum. Models of human lung airways and their application to inhaled particle deposition. *Bull. Math. Biol.* **42**:461–480 (1980).

25. J. S. Fleming, J. H. Conway, S. T. Holgate, E. A. Moore, A. H. Hashish, A. G. Bailey, and T. B. Martonen. Evaluation of the accuracy and precision of lung aerosol deposition measurements from planar radionuclide imaging using simulation. *Phys. Med. Biol.* **43**:2423–2429 (1998).
26. P. R. Phipps, I. Gonda, S. D. Anderson, D. Bailey, and G. Bautovich. Regional deposition of saline aerosols of different tonicities in normal and asthmatic subjects. *Eur. Respir. J.* **7**:1474–1482 (1994).
27. Q. A. Summers, J. S. Fleming, Y. Dai, S. Perring, R. Honeywell, K. J. Gough, A. G. Renwick, A. R. Clark, M. A. Nassim, and S. T. Holgate. The pulmonary deposition of two aerosol preparations of nedocromil sodium delivered by MDI assessed by single photon emission computed tomography. *J. Aerosol Med.* **9**:S93–S109 (1996).
28. J. S. Fleming, A. H. Hashish, J. H. Conway, M. A. Nassim, S. T. Holgate, P. Halson, E. Moore, A. G. Bailey, and T. B. Martonen. Assessment of deposition of inhaled aerosol in the respiratory tract of man using three-dimensional multimodality imaging and mathematical modeling. *J. Aerosol Med.* **9**:317–327 (1996).
29. G. C. Smaldone, R. J. Perry, W. D. Bennett, M. S. Messina, J. Zwang, and J. Ilowite. Interpretation of "24 hour lung retention" in studies of mucociliary clearance. *J. Aerosol Med.* **1**:11–20 (1988).
30. J. E. Agnew, D. Pavia, and S. W. Clarke. Airways penetration of inhaled aerosol: an index to small airways function? *Eur. J. Respir. Dis.* **62**:239–255 (1981).
31. J. Sanchis, M. Dolovich, R. Chalmers, and M. Newhouse. Quantitation of regional aerosol clearance in the normal human lung. *J. Appl. Physiol.* **33**:757–762 (1972).
32. A. P. Greening, M. Miniati, and F. Fazio. Regional deposition of aerosols in health and in airways obstruction: a comparison with krypton-81m ventilation scanning. *Bull. Eur. Physiopathol. Respir.* **16**:287–298 (1980).
33. M. D. Short, D. J. Dowsett, P. J. D. Heaf, D. Pavia, and M. L. Thomson. A comparison between monodisperse Tc-99m-labeled aerosol particles and krypton-81m for the assessment of lung function. *J. Nucl. Med.* **20**:194–200 (1979).
34. D. D. Wilkey, P. S. Lee, F. J. Hass, T. R. Gerrity, D. B. Yeates, and R. V. Lourenco. Mucociliary clearance of deposited particles from the human lung: intra- and inter-subject reproductivity, total and regional lung clearance, and model comparisons. *Arch. Environ. Health* **35**:294–303 (1980).
35. W. M. Foster, E. Langenback, and E. H. Bergofsky. Measurement of tracheal and mucus velocities in man: relation to lung clearance. *J. Appl. Physiol.* **48**:965–971 (1980).
36. E. R. Weibel. *Morphometry of the Human Lung*, Academic Press, New York, 1963.
37. J. W. Logus, M. Trajan, H. R. Hooper, B. C. Lentle, and S. F. P. Mann. Single photon emission tomography of lungs imaged with Tc-labeled aerosol. *J. Can. Assoc. Radiol.* **35**:133–138 (1984).
38. S. Perring, Q. Summers, J. S. Fleming, M. A. Nassim, and S. T. Holgate. A new method of quantification of the pulmonary regional distribution of aerosols using combined CT and SPECT and its application to nedocromil sodium administered by metered dose inhaler. *Br. J. Radiol.* **67**:46–53 (1994).
39. M. S. Berridge and D. L. Heald. *In vivo* characterization of inhaled pharmaceuticals using quantitative positron emission tomography. *J. Clin. Pharmacol.* **39**:25S–29S (1999).
40. M. Dolovich, C. Nahmias and G. Coates. Unleashing the PET: 3D imaging of the lung. In P. Byron, R. Dalby, and S. Farr (eds.), *Respiratory Drug Delivery VII*, Serentec Publishers, Raleigh, 2000, pp. 215–230.
41. J. S. Fleming, A. H. Hashish, J. H. Conway, R. Hartley-Davies, M. A. Nassim, M. J. Guy, J. Coupe, S. T. Holgate, E. Moore, A. G. Bailey, and T. B. Martonen. A technique for simulating radionuclide images from the aerosol deposition pattern in the airway tree. *J. Aerosol Med.* **10**:199–212 (1997).